Advanced Composite Materials
Publication details, including instructions for authors and subscription information:
http://www.tandfonline.com/loi/tacm20

Experimental characterization of microscopic damage progress in quasi-isotropic CFRP laminates: effect of interlaminar-toughened layers

Nobuo Takeda [a] , Satoshi Kobayashi [b] , Shinji Ogihara [c] & Akira Kobayashi [d]

[a] Center for Collaborative Research, The University of Tokyo, 4-6-1 Komaba, Meguro-ku, Tokyo 153, Japan

[b] Graduate Student, The University of Tokyo, Japan

[c] Department of Mechanical Engineering, Science University of Tokyo, 2641 Yamazaki, Noda, Chiba 278, Japan

[d] Department of Mechanical Engineering, Science University of Tokyo, 2641 Yamazaki, Noda, Chiba 278, Japan

Version of record first published: 02 Apr 2012.

To cite this article: Nobuo Takeda , Satoshi Kobayashi , Shinji Ogihara & Akira Kobayashi (1998): Experimental characterization of microscopic damage progress in quasi-isotropic CFRP laminates: effect of interlaminar-toughened layers, Advanced Composite Materials, 7:2, 183-199

To link to this article: http://dx.doi.org/10.1163/156855198X00138

Adv. Composite Mater., Vol. 7, No. 2, pp. 183–199 (1998)

Experimental characterization of microscopic damage progress in quasi-isotropic CFRP laminates: effect of interlaminar-toughened layers

NOBUO TAKEDA,[1] SATOSHI KOBAYASHI,[2] SHINJI OGIHARA[3,*] and AKIRA KOBAYASHI[3]

[1]*Center for Collaborative Research, The University of Tokyo, 4-6-1 Komaba, Meguro-ku, Tokyo 153, Japan*
[2]*Graduate Student, The University of Tokyo, Japan*
[3]*Department of Mechanical Engineering, Science University of Tokyo, 2641 Yamazaki, Noda, Chiba 278, Japan*

Received 18 December 1996; accepted 8 October 1997

Abstract—Microscopic damage progress under static tensile loading in quasi-isotropic CFRP laminates was observed by an optical microscope and a scanning acoustic microscope (SAM). Material systems used were toughened-type CFRP, T800H/3631 and newly developed CFRP with interlaminar-toughened layers, T800H/3900-2. The laminate configurations were quasi-isotropic $[0/45/90/-45]_{s2}$ for T800H/3631 and $[0/45/90/-45]_s$ for T800H/3900-2. Both plain specimens and specimens with a circular hole were tested. By the edge observation of the plain specimens, transverse crack density was measured as a function of laminate strain. The effect of interlaminar-toughened layers on the behavior of the microscopic damage was clarified experimentally. By the SAM observation of specimens with a hole, delamination onset and growth were detected. To discuss the delamination onset from the edge of the open hole, the energy release rate associated with delamination growth was calculated following O'Brien and Raju. The energy release rate predictions of delamination onset and growth was qualitatively consistent with the experimental observation.

Keywords: CFRP; delamination; energy release rate; quasi-isotropic laminates; transverse crack; scanning acoustic microscopy.

1. INTRODUCTION

Carbon fiber reinforced plastics (CFRP) are remarkable for their high specific modulus and strength. This material is usually used in the shape of multidirectional laminates. In the failure process in CFRP laminates, unique microscopic damages, such as transverse cracks and delaminations occur. It is important to understand the behavior of microscopic damages.

*To whom correspondence should be addressed.

O'Brien [1] conducted static and fatigue tensile tests for quasi-isotropic CFRP laminate plain specimens. Delamination onset and growth were observed by X-ray radiography. He derived the energy release rate associated with straight free-edge delamination by using the classical lamination theory. O'Brien and Raju [2] extended the analysis to the delamination onset from an open hole in a composite laminate.

Masters and Reifsnider [3] observed multiplication of transverse cracks in quasi-isotropic CFRP laminates under tensile loading by using the replica technique. It was found that transverse crack spacing saturates before the final fracture of the laminates. They explained the saturated crack spacing by using the shear-lag analysis. Crossman and Wang [4] found that onset and growth of transverse cracks and delaminations in $[\pm 25/90_n]_s$ laminates depend on the thickness of 90° ply. As listed above, the experimental observations of damage progress in quasi-isotropic CFRP laminates have been conducted, but the modeling of damage progress is not yet well established.

On the other hand, it is pointed out that CFRP has low interlaminar fracture toughness. To overcome this problem, some methods to toughen laminates are suggested. One of them is 'interleaving', that refers to sandwiching thin layers of resin between the plies [5–8]. The second approach is to utilize good processability of thermoset resin and high fracture toughness of thermoplastic resin. This hybridization of thermoset and thermoplastic resins is achieved by dispersing particulate thermoplastic polymer into thermoset base resin. One example of these material systems is T800H/3900-2 which is used in the present study.

Odagiri *et al.* [9, 10] showed that T800H/3900-2 laminates provided both high compressive strength after impact damage and high compressive strength at elevated temperatures for moistured test specimens. This was achieved by the heterogeneous interlaminar-toughened layers, introducing fine particles composed of amorphous polyamide onto the prepregs. The delamination growth was suppressed to a great extent by introducing the interlaminar-toughened layers.

Investigations of the enhancement of interlaminar fracture toughness or impact resistance of interleaved or hybridized laminates have been conducted. However, few studies of the failure process of these laminates have been conducted [11].

In the present study, microscopic damage progress in quasi-isotropic CFRP laminates under static tensile loading is investigated. The observation of the damages were conducted by an optical microscope and a scanning acoustic microscope (SAM). To discuss the effect of interlaminar-toughened layers, two material systems were used. Both plain specimens and specimens with a circular hole were tested.

2. EXPERIMENTAL PROCEDURE

2.1. Materials

The materials used were toughened-type CFRP composite T800H/3631, and newly developed CFRP with interlaminar-toughened layers, T800H/3900-2, supplied by

Table 1.
Material properties

Material system	T800H/3631	T800H/3900-2
Longitudinal Young's modulus (GPa)	148	143
Transverse Young's modulus (GPa)	9.57	7.99
In-plane shear modulus* (GPa)	4.50	3.96
In-plane Poisson's ratio*	0.356	0.345
Transverse tensile strength (MPa)	74.2	71.6
Transverse ultimate strain (%)	0.84	0.99

*Assumed value.

Toray Inc. The T800H/3900-2 prepreg system has tough and fine polyamide particles on its surfaces, which results in formation of the interlaminar-toughened layers at every ply interface in the laminates. The thickness of the interlaminar-toughened layers is about 30 μm. Material properties are shown in Table 1 [12]. In-plane shear modulus and in-plane Poisson's ratio are assumed values which are in need for the delamination analysis. The matrix base resin in T800H/3900-2 is very similar to that in T800H/3631.

The laminate configurations were quasi-isotropic $[0/45/90/-45]_{S2}$ ($[0/45/90/-45_2/90/45/0_2/45/90/-45_2/90/45/0]$) for T800H/3631 and $[0/45/90/-45]_S$ ($[0/45/90/-45_2/90/45/0]$) for T800H/3900-2. Specimen configuration is shown in Fig. 1. Plain specimens and specimens with a circular hole were prepared. The specimens with a circular hole had a hole whose diameter was 10 mm at the center. The fiber volume fraction was about 64% for T800H/3631, and 55% for T800H/3900-2. The low fiber volume fraction in T800H/3900-2 is due to the introduction of interlaminar-toughened layers. GFRP tabs were glued on the specimens.

2.2. *Damage observation*

Quasi-static tensile tests were performed at room temperature. The cross-head speed was 0.5 mm/min.

By the observation of polished edge of the plain specimens, damage progress was measured as a function of laminate strain. During the tests, the testing machine was periodically stopped, and the specimens were observed by an optical microscope directly. The observed area was 50 mm long at the center of the specimens. The number of transverse cracks in the specimen was counted to obtain the transverse crack density, which was defined as the number of transverse cracks per unit specimen length.

Both plain specimens and specimens with a hole were also observed by a scanning acoustic microscope (SAM, Olympus UH-3, Pulse-Wave Mode, 30 MHz, HA lens [13]) to detect delamination onset and growth. High resolution images including transverse cracks can be observed by introducing transverse waves as well as longitudinal ones in composite laminates.

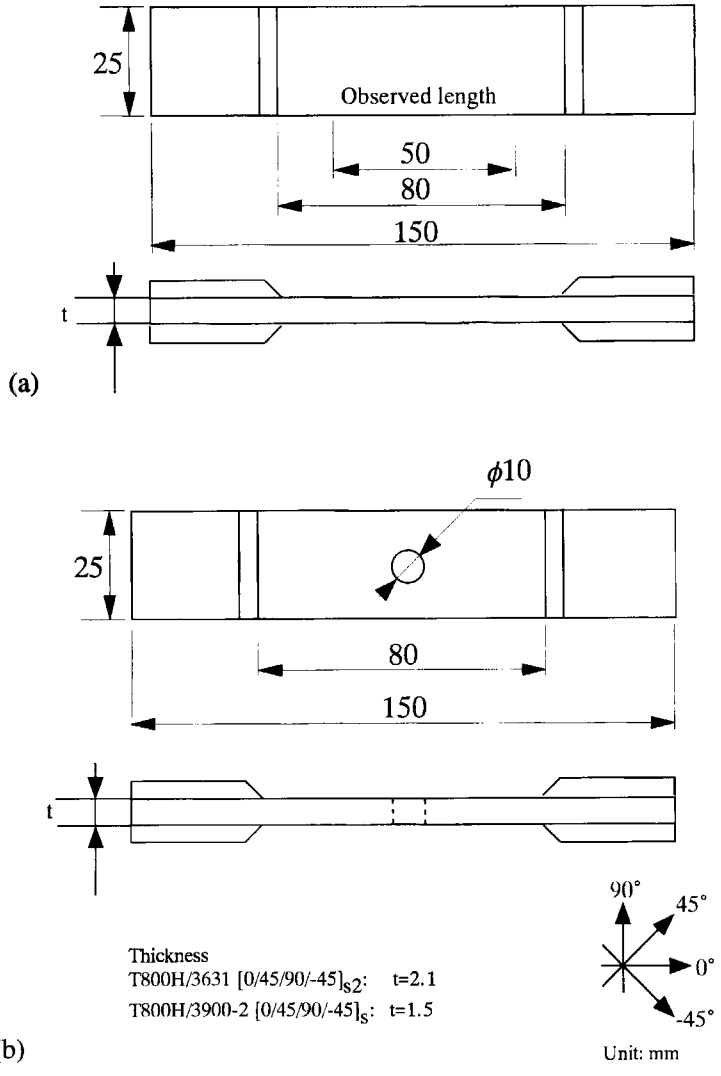

Figure 1. Specimen configurations of test specimen: (a) plain specimens; (b) specimens with a circular hole.

3. RESULTS

3.1. Plain specimens

Laminate properties obtained from tensile tests are shown in Table 2. The lower Young's modulus in T800H/3900-2 than that of T800H/3631 is due to the lower fiber volume fraction. Both laminates have almost the same tensile strength, however, T800H/3900-2 laminates have higher ultimate strain than T800H/3631 laminates.

Figure 2 shows edge damage state in a T800H/3631 plain specimen ((a) $\varepsilon = 1.12\%$, (b) $\varepsilon = 1.39\%$, ε = laminate strain). In Fig. 2a, a transverse crack in 90° ply is

Table 2.
Properties of plain specimens

Laminates	T800H/3631 $[0/45/90/-45]_{s2}$	T800H/3900-2 $[0/45/90/-45]_s$
Tensile strength (MPa)	794	799
Young's modulus (GPa)	58.9	52.8
Ultimate strain (%)	1.38	1.48

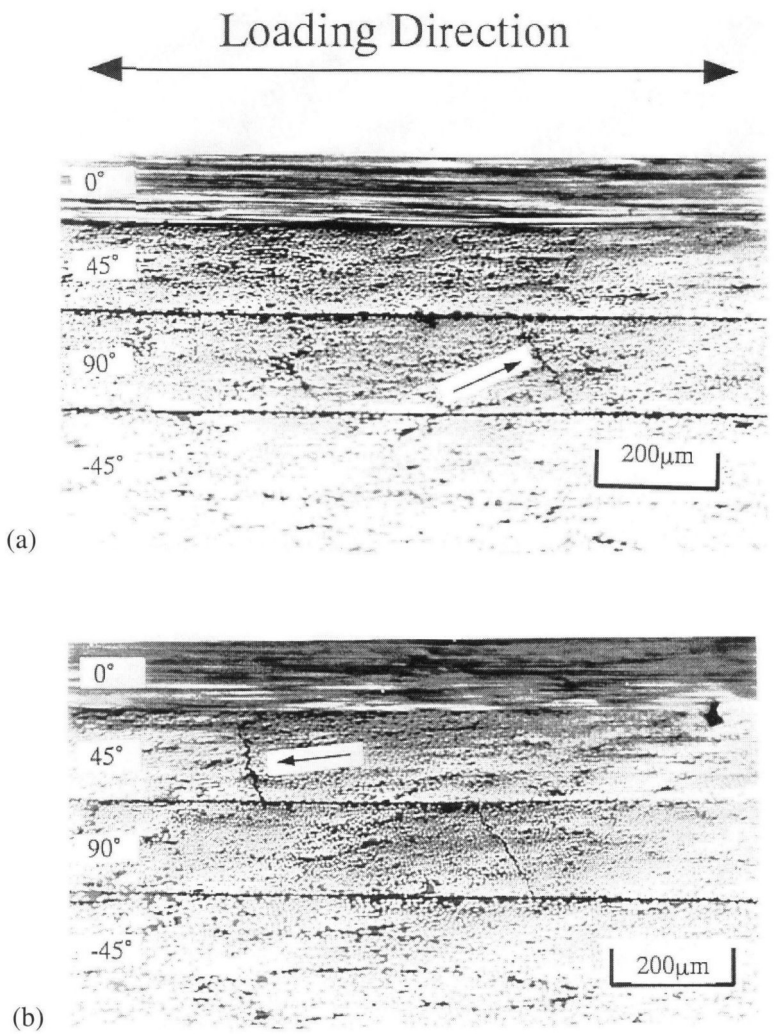

Figure 2. Damage progress in a T800H/3631 $[0/45/90/-45]_{s2}$ plain specimen: (a) $\varepsilon = 1.12\%$; (b) $\varepsilon = 1.39\%$ (ε: laminate strain).

observed. In Fig. 2b, new transverse crack in 45° ply is observed at higher strain. In this specimen, the first microscopic damage observed was transverse crack in 90° ply. At higher strain levels, transverse cracks in 45° and −45° plies were observed. Transverse cracks in −45° plies always ran through the thickness of two adjacent −45° plies. As the laminate strain increased, the number of cracks in each ply increased.

Just before the final fracture, free edge delamination at 45/90 interface from transverse crack tips were observed. Figure 3 shows delamination at 45/90 interface observed by a scanning acoustic microscope (SAM, Pulse-Wave Mode, HA lens, 30 MHz). The white area indicated by the arrows correspond to delaminations. The intensity of reflected acoustic wave from delaminated area is larger which results in a formation of the white area. By the combination of the edge observation, it was found that the delaminations occurred from the tips of the transverse cracks at 45/90 interface. Extensive growth of delaminations was not observed because the final fracture of the laminate occurred.

Figure 4 shows edge damage state in a T800H/3900-2 plain specimen ((a) $\varepsilon = 1.01\%$, (b) $\varepsilon = 1.49\%$). Interlaminar-toughened (polyamide particle-dispersed) layers are observed at every ply interface. The behavior of transverse cracks in each layer in this specimen is similar to that in T800H/3631 specimens. That is, the first transverse crack is observed in 90° ply, and then, in 45° and −45° plies. In this specimen, delamination was not observed, which is due to the enhancement of interlaminar fracture toughness supplied by the interlaminar-toughened layers.

As shown in Figs 2 and 4, the surface of the transverse cracks in 90° plies were not perpendicular to the loading direction. Figure 5a shows a schematic illustration of transverse cracks observed from both edges. This inclination of transverse crack

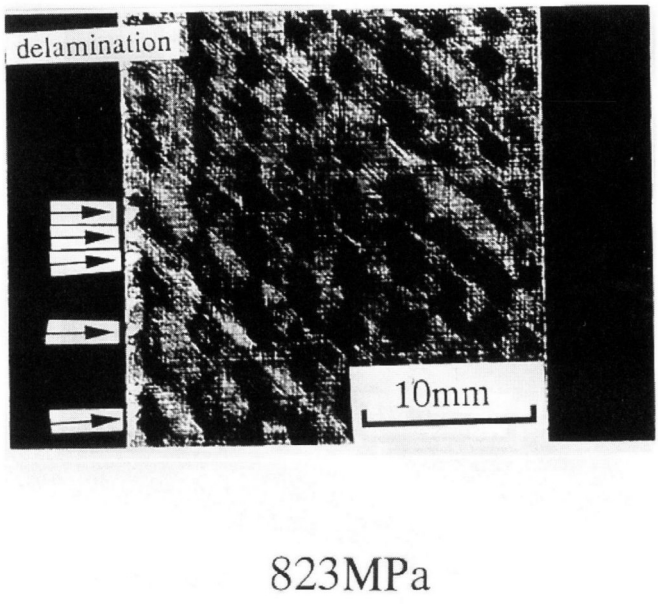

Figure 3. Delamination in a T800H/3631 $[0/45/90/-45]_{s2}$ plain specimen at $\varepsilon = 1.28\%$.

surface in the 90° ply is attributed to the cross-elasticity effect of adjacent off-axis plies (Fig. 5b) which result in generation of shear stress in 90° plies (Fig. 5c).

Figures 6 and 7 show the transverse crack density as a function of the laminate strain for T800H/3631 and T800H/3900-2 specimens, respectively. The transverse crack density is defined as the number of cracks in a ply per centimeter. There are four and two 90° (45°) plies in T800H/3631 and T800H/3900-2 specimens, respectively. Transverse crack density was measured for each ply, but transverse crack density for the plies with the same fiber orientation was very similar. Therefore, the average values were plotted in Figs 6 and 7. The two adjacent −45° plies were treated as one ply, because the transverse cracks in this ply always ran through the thickness of the two −45° plies.

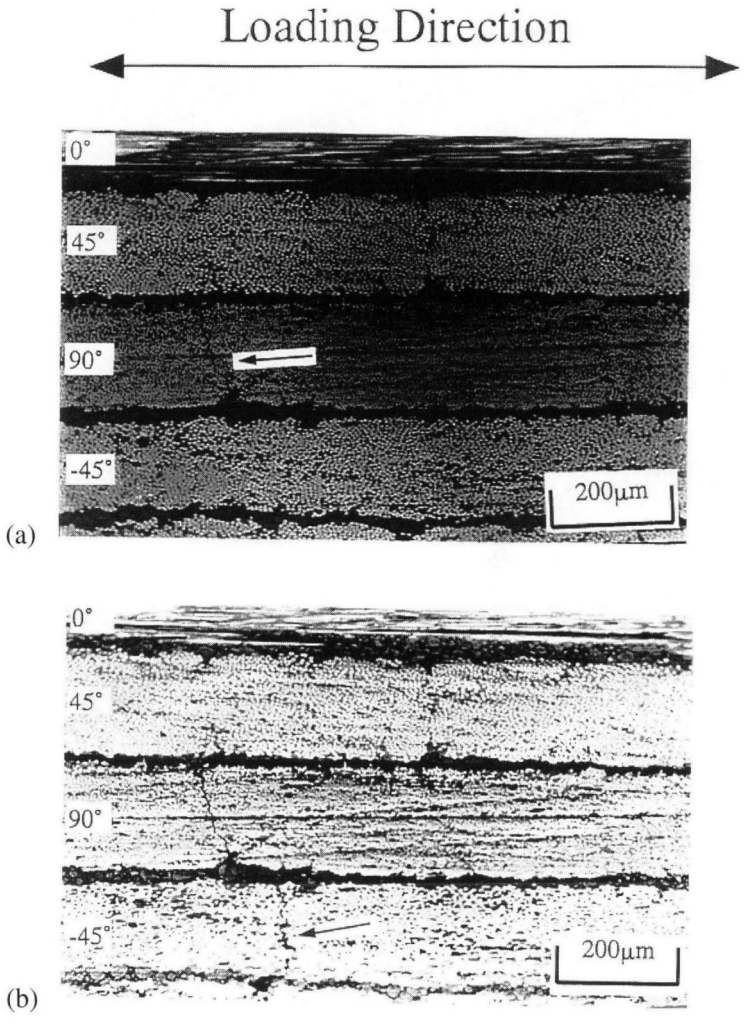

Figure 4. Damage progress in a T800H/3900-2 $[0/45/90/-45]_{s2}$ plain specimen: (a) $\varepsilon = 1.01\%$; (b) $\varepsilon = 1.49\%$.

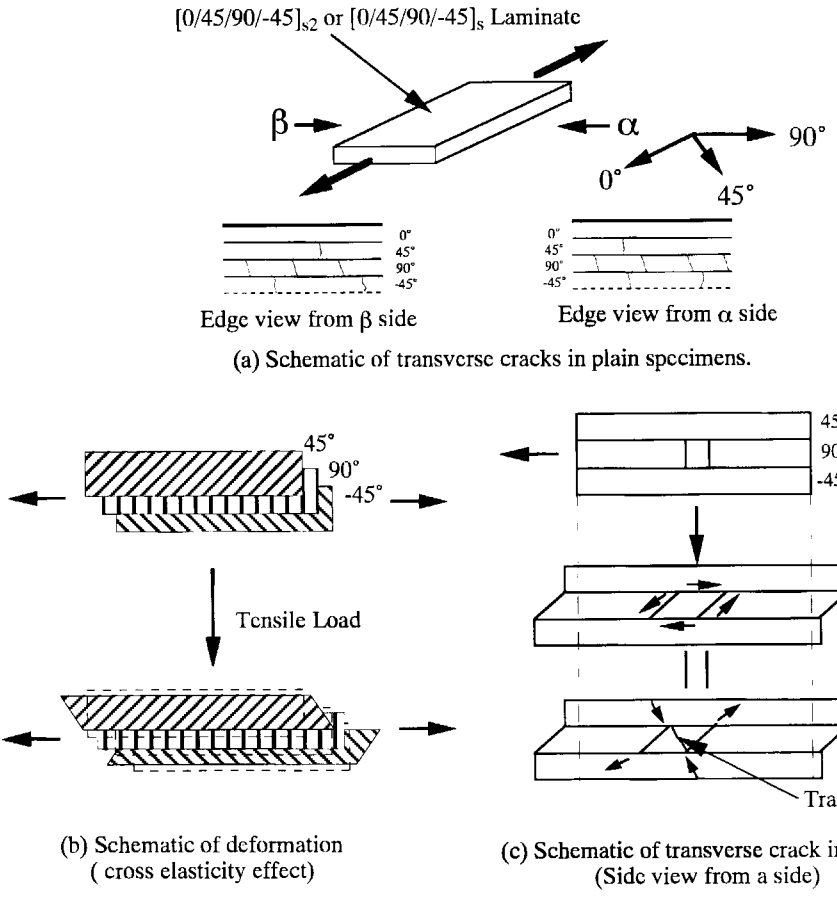

Figure 5. Schematic of transverse crack formation in plain specimens.

The onset strain of transverse cracks in the 90° ply in T800H/3900-2 is smaller than that in T800H/3631. This can not be explained by the transverse ultimate strain for each lamina listed in Table 1. It is necessary to consider the thermal residual strain and the shear stress generated by the cross-elasticity effect. The onset strain of transverse cracks in the 45° and −45° plies for T800H/3900-2 is larger than for those in T800H/3631. This may be partly because of the reduction of in-plane shear stress in 45° and −45° plies by introducing the interlaminar-toughened layers. In both material systems, transverse crack density in the −45° ply is higher than that in the 45° ply. This is the effect of the difference in thermal residual strain which is due to the difference in thickness of the −45° ply group and +45° ply.

3.2. Specimens with a circular hole

Stresses at final fracture of the specimen with a hole obtained from tensile tests are shown in Table 3. For a plain specimen, T800H/3900-2 laminates have higher tensile strength and ultimate strain than T800H/3631 laminates; however, for specimens

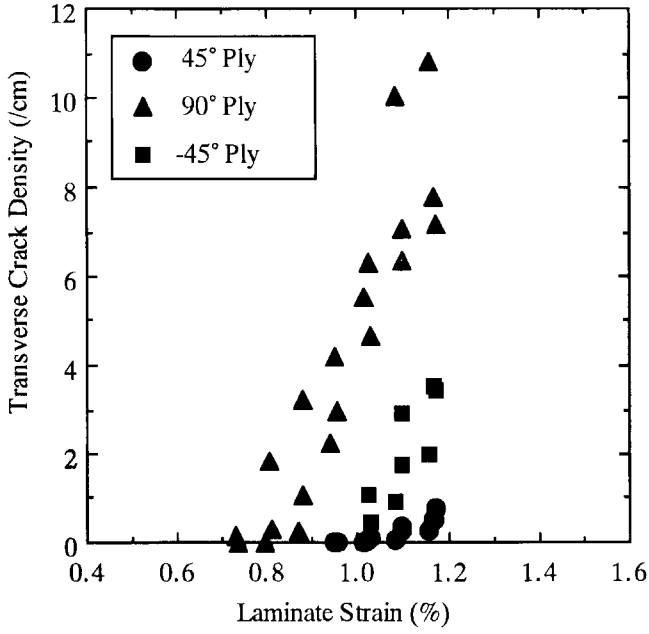

Figure 6. Transverse crack density as a function of laminate strain in T800H/3631 $[0/45/90/-45]_{s2}$ plain specimens.

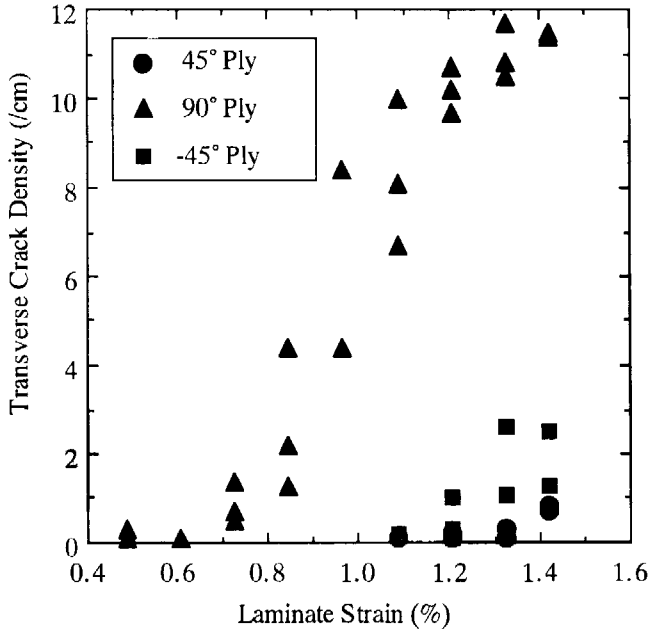

Figure 7. Transverse crack density as a function of laminate strain in T800H/3900-2 $[0/45/90/-45]_s$ plain specimens.

Table 3.
Stresses at final fracture of specimens with a hole

Laminates	T800H/3631 $[0/45/90/-45]_{s2}$	T800H/3900-2 $[0/45/90/-45]_s$
Remote tensile stress at final fracture (MPa)	464	335
Average tensile stress in the minimum net cross-section (MPa)	784	566

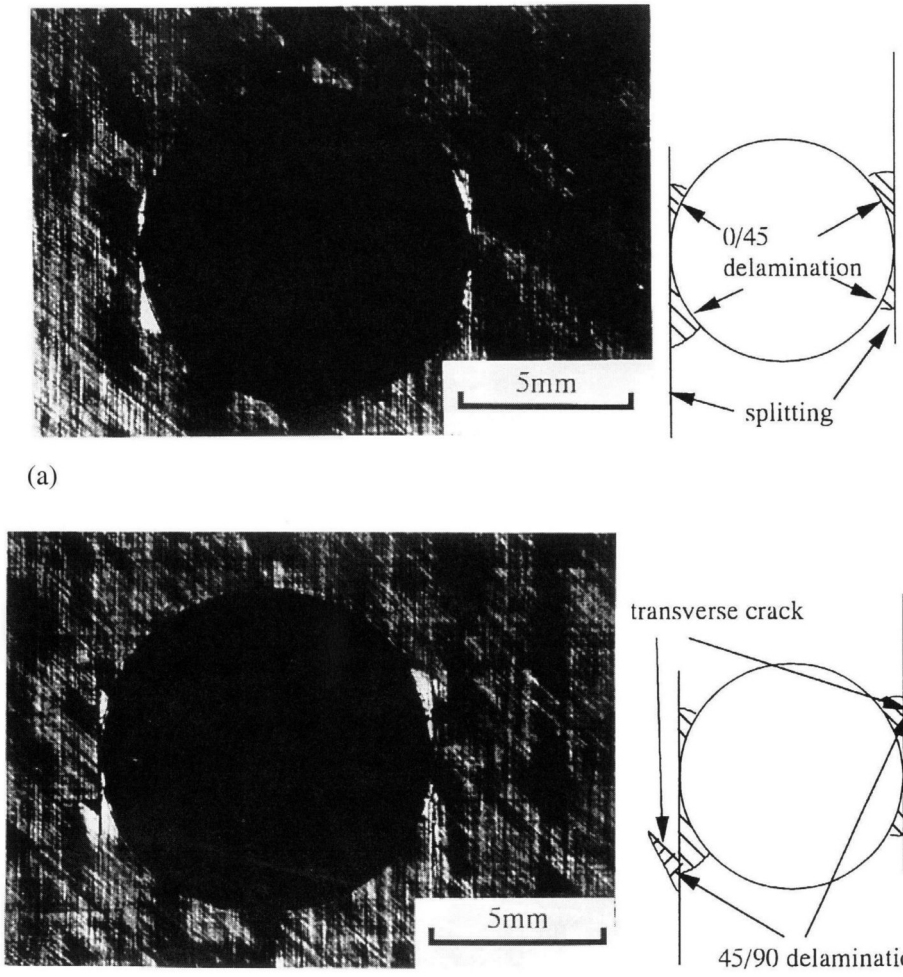

Figure 8. SAM image (30 MHz HA pulse lens) of T800H/3631 $[0/45/90/-45]_{s2}$ specimen with a circular hole: (a) $\sigma = 294$ MPa; (b) $\sigma = 343$ MPa; (c) $\sigma = 412$ MPa; (d) $\sigma = 450$ MPa (σ: remote stress).

with a hole, T800H/3631 have higher strength. It should be noted that the laminate configuration is different between these material systems. It is considered that the T800H/3631 $[0/45/90/-45]_{s2}$ laminate has two 0° plies in the middle of the laminate. It is considered that the 0° ply group reduces the notch sensitivity (the net of the strength of the specimens with a hole to that of plain specimens). To compare the notch sensitivity between the two laminates, it is necessary to test material systems with the same laminate configuration.

In the T800H/3631 specimens with a hole, delamination onset and growth around the hole was observed as shown in Fig. 8. First, longitudinal splitting occurred from the edge of an open hole and delamination occurred at near 70°, 110°, 250° and 290° at 0/45 interface (Fig. 8a, $\sigma = 294$ MPa, σ: remote tensile stress). As the

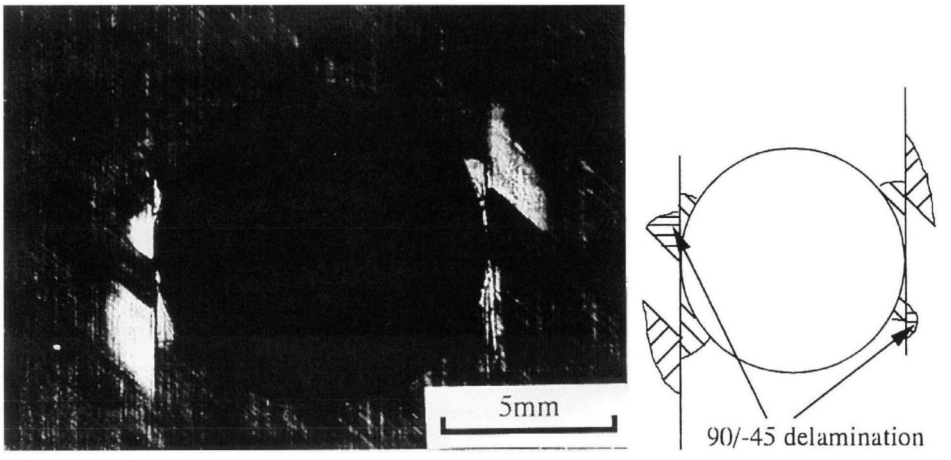

(c)

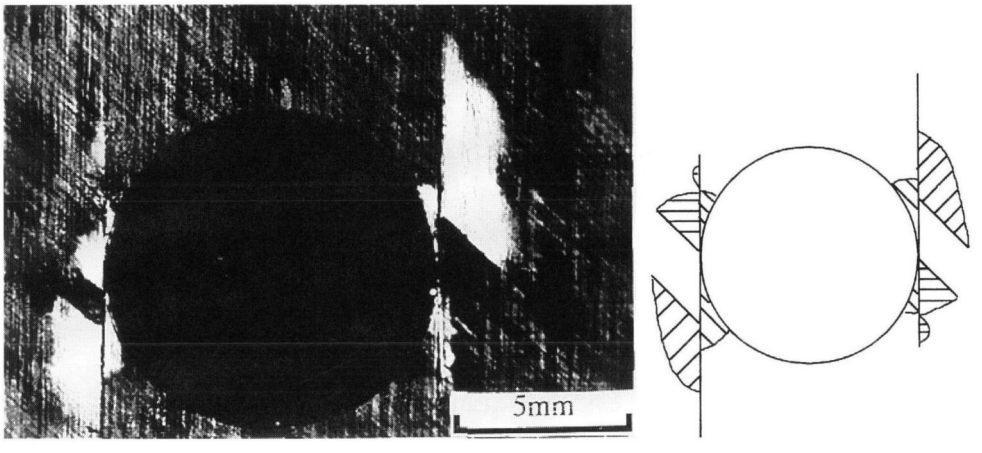

(d)

Figure 8. (Continued).

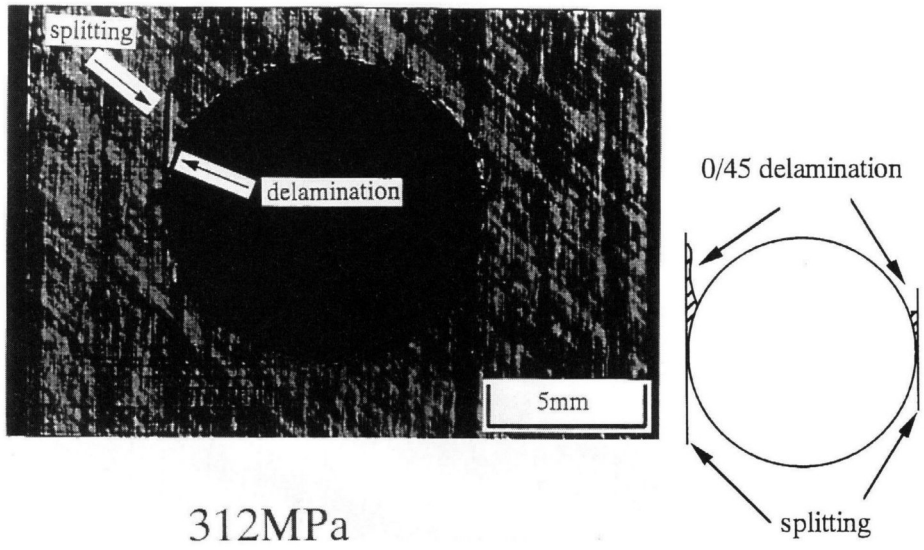

Figure 9. SAM image (30 MHz HA pulse lens) of T800H/3900-2 $[0/45/90/-45]_s$ specimen with a circular hole ($\sigma = 312$ MPa).

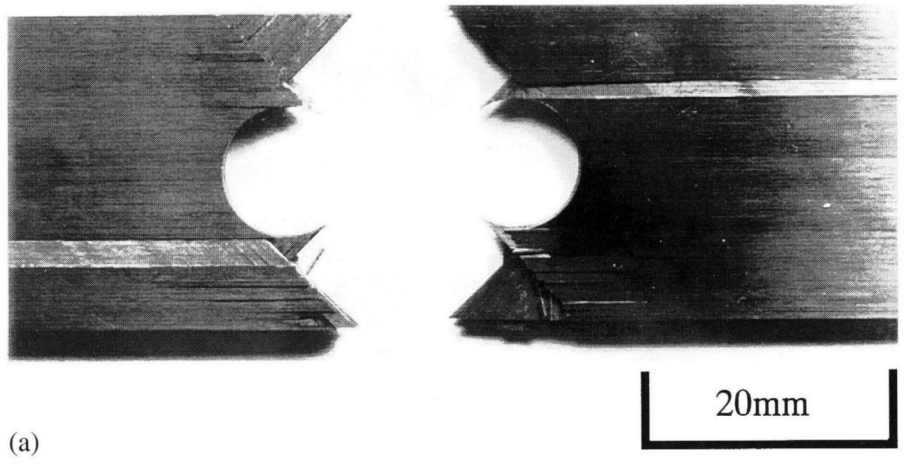

Figure 10. Specimen with a circular hole after final fracture: (a) T800H/3631 $[0/45/90/-45]_{s2}$; (b) T800H/3900-2 $[0/45/90/-45]_s$.

laminate strain increased, delamination onset at near 120° and 300° at 45/90 interface (Fig. 8b, $\sigma = 343$ MPa), and near 90°, 120°, 270° and 300° at 90/−45 interface (Fig. 8c, $\sigma = 412$ MPa). Delamination at 45/90 interface grew extensively (Fig. 8d, $\sigma = 450$ MPa).

Figure 9 shows delamination in the T800H/3900-2 specimen, ($\sigma = 312$ MPa). First, the longitudinal splitting from the edge of an open hole occurred in the 0° ply. Then delamination at the 0/45 interface occurred around the longitudinal splitting. Extensive growth of the delamination was not observed. This is due to the high in-

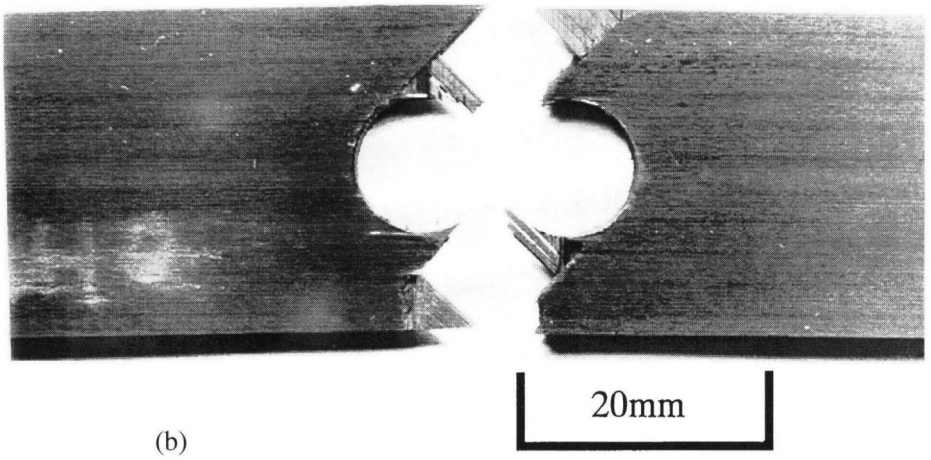

Figure 10. (Continued).

terlaminar toughness created by the interlaminar-toughened layers. Delaminations at the 0/45 interface were caused by stress concentration around the tip of the longitudinal splitting. Delaminations at other interfaces were not observed. Final fracture of the laminate occurred by instant coalescence of transverse cracks and delaminations induced by the transverse cracks.

Figure 10 shows specimens after final fracture for both material systems. Delamination area in T800H/3631 is larger than that in T800H/3900-2. This also indicates the effect of high interlaminar toughness supplied by the interlaminar-toughened layers.

4. DISCUSSION

O'Brien [1] derived an equation for the energy release rate associated with straight-edge delamination growth, G, as

$$G = \frac{\varepsilon^2 t}{2m}\left(E_{\mathrm{LAM}} - E^*\right), \tag{1}$$

where ε is the nominal strain, t is the laminate thickness, m is the number of delaminations formed, and E_{LAM} and E^* are the laminate modulus before and after delamination. It is known that the energy release rate associated with edge delamination growth increases as the delamination length increases and reaches the value of equation (1).

O'Brien and Raju [2] extended the analysis to the delamination onset from an open hole in a composite laminate and derived the energy release rate associated with delamination onset around an open hole, $G(\theta)$ at θ portion from the loading direction. In the present study, we assume that the loading direction is 0° and that

counterclockwise is the positive direction. $G(\theta)$ is expressed as

$$G(\theta) = (1 - 2\cos 2\theta)^2 \varepsilon_0^2 \frac{t}{2m}\left[E_{\mathrm{LAM}} - E^*(\theta)\right], \tag{2}$$

where E_{LAM} and $E^*(\theta)$ are the laminate modulus before and after delamination at the θ portion modeled as a straight edge and ε_0 is the remote tensile strain. Hence, with a remote tensile stain of ε_0, G will vary with θ due to the variation in circumferential strain as well as the variation in laminate modulus after delamination, E^*. Therefore, equation (2) was normalized to yield

$$\frac{G}{\varepsilon_0^2} = \frac{t(1 - 2\cos 2\theta)^2}{2m}\left[E_{\mathrm{LAM}} - E^*(\theta)\right]. \tag{3}$$

Figure 11 shows the distribution of normalized energy release rate associated with the delamination growth calculated by equation (3). The values are plotted in the radial direction for each θ portion. Material properties used in the analysis are listed in Table 1. Although the maximum value of normalized energy release rate in T800H/3900-2 is larger than that in T800H/3631, only a little delamination was observed in T800H/3900-2. This shows that a large critical energy release rate was achieved by using interlaminar-toughened layers. The energy release rate derived in the above analysis is an asymptotic value for an extended delamination. It is known that the energy release rate associated with edge delamination growth increases and reaches the value of equation (1).

Therefore it is impossible to predict delamination onset by the energy release rate calculated by equations (1) and (2). Here, it is assumed that an inherent flaw which can be regarded as a small delamination exists, and that the energy release rate is larger at the interface where the energy release rate calculated by equations (1) and (2) is larger for a flaw with same length. With the assumption that the delamination occurs at earlier stage where the energy release rate is larger, the order of delamination onset can be predicted.

The order of delamination onset location predicted is shown in Table 4. The order of delamination onset location in T800H/3631 laminates predicted is (1) at 108° and 288° at a 45/90 interface; (2) at 64°, 116°, 244° and 296° at a 0/45 interface; and (3) at 84°, 125°, 264° and 305° at a 90/−45 interface. In the experiments, the order was reversed for the first and the second. This is due to the stress concentration around the tips of the longitudinal splittings in the 0° ply. In T800H/3900-2 laminates, only small delaminations at 0/45 interface were observed which correspond to the delamination of third order in the prediction. This is also due to the stress concentration around the longitudinal splittings.

As shown in Fig. 8, the most extensive growth of delamination is observed at the 45/90 interface. The locations are near the locations where the energy release rate calculated by equation (3) is maximum (45/90 interface 108°, 288°, see Table 4 and Fig. 11). For a quantitative characterization of delamination growth, it is necessary to estimate mode I, II and III components of the energy release rates. In addition, the delamination growth criterion must be established.

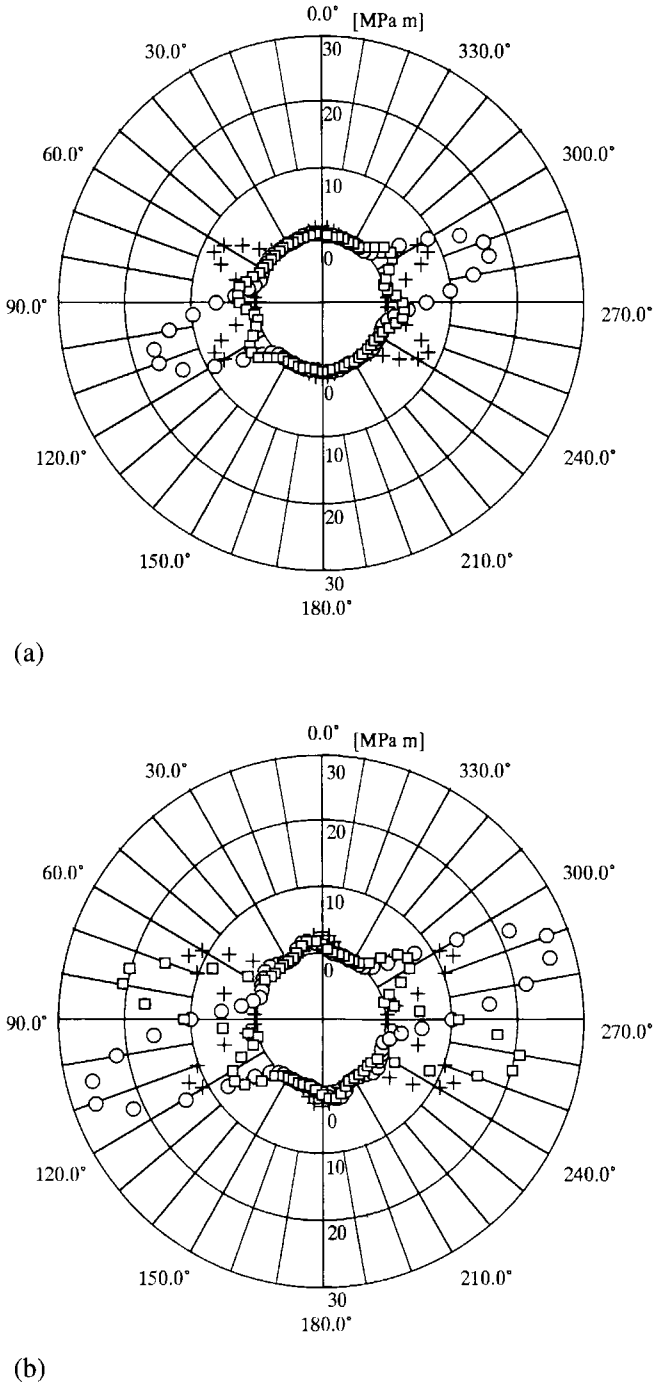

Figure 11. Normalized energy release rate associated with delamination growth in specimen with a circular hole: (a) T800H/3631 $[0/45/90/-45]_{s2}$; (b) T800H/3900-2 $[0/45/90/-45]_s$ ((+) [0/45] interface; (○) [45/90] interface; (□) [90/−45] interface).

Table 4.
The order of delamination onset (prediction and experimental results)

T800H/3631 $[0/45/90/-45]_s$		
	Prediction	Result
(1)	45/90 interface 108°, 288°	0/45 interface 70°, 110°, 250°, 290°
(2)	0/45 interface 64°, 116°, 244°, 296°	45/90 interface 120°, 300°
(3)	90/−45 interface 84°, 125°, 264°, 305°	90/−45 interface 90°, 120°, 270°, 300°
T800H/3900-2 $[0/45/90/-45]_s$		
	Prediction	Result
(1)	45/90 interface 108°, 288°	0/45 interface 70°, 110°, 250°, 290°
(2)	90/−45 interface 78°, 258°	
(3)	0/45 interface 65°, 115°, 245°, 295°	
(4)	90/−45 interface 124°, 304°	

Although the analysis does not consider the thermal residual stress generated during the curing process, the prediction is useful for predicting the location of the delamination onset.

5. CONCLUSION

Microscopic damage progress under static tensile loading in quasi-isotropic CFRP laminates with and without interlaminar-toughened layers was observed by an optical microscope and a scanning acoustic microscope (SAM).

(1) By the edge observation of the plain specimens, transverse crack density was measured as a function of laminate strain.

(2) By the SAM observation of specimens with a circular hole, delamination onset and growth were detected.

(3) The energy release rate analysis conducted by O'Brien and Raju can be used for qualitative prediction of delamination onset and growth.

REFERENCES

1. O'Brien, T. K. Characterization of delamination onset and growth in a composite laminates. In: *ASTM STP 775*. Am. Soc. for Testing and Mater. (1982), pp. 140–167.
2. O'Brien, T. K. and Raju, I. S. Strain-energy-release rate analysis of delamination around an open hole in composite laminates. *AIAA Journal* **84-0961**, 526–536 (1984).

3. Masters, J. E. and Reifsnider, K. L. An investigation of cumulative damage development in quasi-isotropic graphite/epoxy laminates. In: *ASTM STP 775*. Am. Soc. for Testing and Mater. (1982), pp. 40–61.
4. Crossman, F. W. and Wang, A. S. D. The dependence of transverse cracking and delamination on ply thickness in graphite/epoxy laminates. In: *ASTM STP 775*. Am. Soc. for Testing and Mater. (1982), pp. 119–139.
5. Chan, W. S., Rogers, C. and Aker, S. Improvement of edge delamination strength of composite laminates using adhesive layers. In: *ASTM STP 893*. Am. Soc. for Testing and Mater. (1986), pp. 266–285.
6. Norman T. L. and Sun, C. T. Mechanical properties and interlaminar toughness of cross-plied laminates containing adhesive strip. *AIAA Journal* **29**, 247–252 (1991).
7. Ozdil, F. and Carlsson, L. A. Plastic zone estimates in mode I interlaminar fracture of interleaved composites. *Eng. Fract. Mech.* **41**, 645–658 (1992).
8. Aksoy, A. and Carlsson, L. A. Interlaminar shear fracture of interleaved graphite/epoxy composite. *Compos. Sci. Technol.* **43**, 55–69 (1992).
9. Odagiri, N., Muraki, T. and Tobukuro, K. Toughness improved high performance TORAYCA prepreg T800H/3900 series. In: *33rd Int. SAMPE Symposium*. Anaheim, CA (1988), pp. 272–283.
10. Odagiri, N., Kishi, H. and Nakane, T. T800H/3900-2 toughened epoxy prepreg system: toughening concept and mechanism. In: *The American Society for Composites, 6th Technical Conference*. Troy, NY (1991), pp. 46–52.
11. Altus, E. and Ishai, O. The effect of soft interleaved layers on the combined transverse cracking/delamination mechanisms in composite laminates. *Compos. Sci. Technol.* **39**, 13–27 (1990).
12. Takeda, N., Niizuma, H., Ogihara, S. and Kobayashi, A. Experimental evaluation of thermal residual stress in CFRP cross-ply laminates. *Materials System* **14**, 73–78 (1995) (in Japanese).
13. Takeda, N., Kosaka, T. and Endo, T. Scanning acoustic microscopy for high-resolution damage detection in anisotropic composites – simulation and experiments. *Japan Int. SAMPE Symposium*. Tokyo (1995), pp. 885–890.